Collisional effects in the stimulated Raman Q branch of O_2 and O_2–N_2 ⊘

G. Millot; R. Saint-Loup; J. Santos; R. Chaux; H. Berger; J. Bonamy

Check for updates

View Online

Export Citation

CrossMark

Collisional effects in the stimulated Raman Q branch of O_2 and O_2–N_2

G. Millot, R. Saint-Loup, J. Santos,[a] R. Chaux, and H. Berger
Laboratoire de Spectronomie Moléculaire et Instrumentation Laser, Université de Bourgogne, U.R.A. CNRS no. 777, 6 Bd Gabriel, 21000. Dijon France

J. Bonamy
Laboratoire de Physique Moléculaire, Université de Franche-Comté, U.R.A. CNRS no. 772, La Bouloie, Route de Gray, 25030 Besançon France

The fundamental isotropic Raman Q branch of oxygen at pressures up to 2 atm and for temperatures between 295 and 1350 K has been recorded using stimulated Raman gain spectroscopy (SRGS) for collisions with oxygen and nitrogen. The line broadening and line shifting coefficients have been determined for several rotational quantum numbers (up to $N = 55$ at 1350 K). The temperature dependence of these coefficients has also been studied for most of the rotational lines. The line parameters (widths and shifts) have been then calculated *a priori* through a semiclassical model. A good agreement between experimental and theoretical data has been observed. Another theoretical approach based on fitting and scaling law has been used to calculate the line broadening coefficients. It is shown that a modified exponential energy gap model (MEG) and an energy corrected sudden law (ECS) for the state-to-state rotationally inelastic rates, account for the rotational and temperature dependences of the observed linewidths. With regard to the energy corrected sudden law, the best results are obtained when the basis rate constants are modeled with a hybrid exponential-power fitting law (EP). The line broadening and shifting coefficients of the oxygen–nitrogen mixture are very close to those found for pure oxygen.

I. INTRODUCTION

It is now well known that coherent anti-Stokes Raman spectroscopy (CARS) is a versatile tool for temperature and concentration measurements in various gaseous systems[1] like burners and combustion engines. In this method, nitrogen is the most frequently used probe molecule due to its abundance and very simple spectroscopic properties. Oxygen which has spectroscopic properties similar to those of nitrogen is also of a special interest as the probe molecule.[2-4] For CARS temperature measurements both rotational and temperature dependences of the pressure broadening coefficients are necessary. Up to now, temperatures were measured from oxygen CARS vibrational spectra[2,3] with the assumption of constant Raman linewidths for all rotational lines. This crude assumption leads to a greater uncertainty in the determination of temperature.[3] To our knowledge, no temperature dependent vibrational Raman linewidths were available up to now. The Q-branch linewidths of oxygen were recently measured[5] by using high resolution CARS, but only for the first nine transitions ($N = 1$–17) and at only one temperature (295 K). So, in order to mitigate the consequence of this lack of knowledge, we have focused our attention on the determination of the line broadening coefficients of pure oxygen over a large temperature range (295–1350 K) and for several rotational quantum numbers. Similar measurements have also been made for the O_2–N_2 mixture.

The aim of our work was to define accurate rotational relaxation models for high pressure and high temperature. The method usually consists of starting with low pressure spectra recorded by stimulated Raman spectroscopy. Then, by using suitable profiles, such as the Galatry profile[6] to take into account Dicke narrowing[7,8] or the Rosenkranz profile[9] to take into account weak overlap between adjacent lines,[10] we obtained the isolated line parameters as a function of the pressure. Two distinct classes of parameters must be considered depending on either the line positions or the linewidths. The line shiftings were deduced from the line frequencies measured at various pressures and then by extrapolation at zero pressure absolute line frequencies were obtained leading to accurate determination of molecular constants.[11] On the other hand, the line broadening coefficients were deduced from the pressure dependence of the linewidths. These shifting and broadening coefficients have been compared with semiclassical calculations[12] over a wide temperature range. The set of broadening coefficients is then inverted to obtain state-to-state rate constants for inelastic collisions by using fitting laws which contain a reduced number of adjustable parameters.[13] Among the various fitting laws, we have tested the modified exponential model (MEG) proposed by Koszykowski and co-workers[14] and the energy corrected sudden scaling law (ECS) proposed by De Pristo and co-workers.[15] In the ECS rate law, the basis rate constants have been taken as a power law (P)[16] and as a hybrid exponential power law (EP).[17] In a recent study,[17] the ECS-EP law has been found to give a very good description of both rotational and temperature dependences of the Raman line broadening coefficients for many collisional systems. In particular, ECS-

---

[a] Present address: Instituto de Estructura de la Materia, CSIC, Serrano 123, 28006 Madrid Spain.

EP accounts for the linewidths of N_2–H_2O contrary to ECS-P.[18] For O_2–O_2 and O_2–N_2, we have found that ECS-EP does not overestimate the linewidths for high rotational quantum number in opposition to ECS-P.

In the following section (Sec. II), we describe the stimulated Raman spectrometer, particularly emphasizing the method performed for the collisional shift measurements. Section III presents the strategy of the measurements and the line shape fitting procedure used to extract line broadening and line shifting coefficients. The experimental results obtained for the line broadening and line shifting coefficients over a wide temperature range (for O_2–O_2 and O_2–N_2) are described in Secs. IV and V, respectively. In Sec. VI, we compared these experimental coefficients with semiclassical calculations. The fitting laws are studied in Sec. VII and a complete set of MEG, ECS-P, and ECS-EP parameters is presented. Finally, Sec. VIII provides the conclusion of this study.

II. EXPERIMENT

The schematic arrangement of the stimulated Raman spectrometer is shown in Fig. 1. We will just recall the main characteristics.[19] The probe beam comes from a single mode Krypton laser frequency stabilized with a Fabry–Perot interferometer. The frequency jitter is then reduced to 1 MHz. Because the Fabry–Perot interferometer is temperature stabilized the slow drift of the laser is reduced to about 30 MHz per hour. The pump source uses a continuous tunable narrow bandwidth dye laser (1 MHz) which is pulse amplified up to 750 kW by four dye cells pumped by a frequency-doubled Nd-YAG laser. A Michelson wave meter[20] provides accurate absolute measurements of both Kr^+ and dye lasers, owing to a reference He–Ne laser stabilized on hyperfine components of $^{127}I_2$. For each spectral scan of the dye laser, only the initial and final wavelengths of both lasers are measured. During the scan, the dye frequency is controlled with a stabilized confocal etalon. Because the drift of the Kr^+ laser during each scan is relatively small (typically 10 MHz), we assumed that its frequency is constant and equal to the average of the initial and final values. An important point concerns the line shifting measurements. Up to now, the line shifts were obtained by measuring the Raman line positions for successive scans at different densities and the frequencies were plotted as a function of densities thanks to a linear law. But this method is not very accurate to measure small line shifting coefficients such as for N_2[21] or O_2 and O_2–N_2 (of the order of -3.5×10^{-3} cm^{-1} atm^{-1} for O_2 at 295 K). So, in order to increase the accuracy of line shift measurements, we have developed on our device a differential method by using a reference cell as shown in Fig. 1. The principle of this method is very simple. Indeed, two spectra are simultaneously recorded within the same experimental conditions: The first one is recorded in the main gas sample at any temperature and pressure, whereas the second one is recorded in the reference cell at constant pressure and temperature. The collisional shift is then derived by comparing the frequencies of the Raman lines obtained in the two channels. For that, the two laser beams are mixed by a dichroic mirror and simultaneously focused into the two cells by passing through a 50% beam splitter. After passing through the cells, the pump beams are stopped, whereas the probe beams arrive on a mechanical chopper, working at 50 Hz and playing two different roles with the following features: it defines the time origin to start the Nd-YAG laser pulses and it modulates the two beams arriving from the two channels through two holes in the disk. The channels are selected by software by adjusting the delay between the beginning of flashes and laser shots. Finally, the two probe beams arrive on the same fast photodiode. During the scanning of the dye laser, the two channels are analyzed one after another; 8–16 shots are usually averaged on each channel. This differential method presents some advantages with respect to the technique consisting in absolute measurements of frequencies in a single channel:
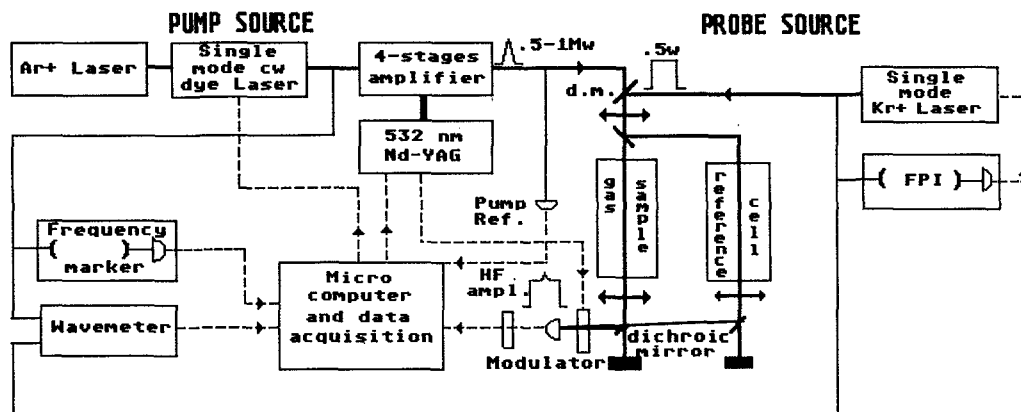

FIG. 1. Schematic diagram of the stimulated Raman spectrometer.

—the problems of frequency calibration are suppressed or less crucial. In particular, the stabilization of the probe laser (Kr$^+$ laser) does not require a high degree of accuracy;

—as the pump beams have approximately the same power in the two channels and are focused in a similar way, the contribution of Stark shift is eliminated. This is a difference with respect to the technique developed by Byschel and Dyer for H$_2$ line shift measurements;[22] in their experiment, a reference cell was located just after the main cell. In this manner, the recorded Raman signal was a combination of two signals that were deconvoluted from each other in the data-fitting procedure. As the focusing in the two cells are not exactly similar, the Stark shift could be not completely eliminated;

—with our method the accuracy of line shift measurement depends only on line shape considerations and signal to noise ratio;

—to measure the collisional shift of a mixture, e.g., O$_2$–N$_2$, it is not necessary to know the contribution of pure oxygen, one only has to put the same pressure of oxygen (at the same temperature) in the two gas cells.

III. MEASUREMENTS STRATEGY AND LINESHAPE FITTING PROCEDURE

Let us recall that the rotational levels in a vibrational state of the $^3\Sigma_g^-$ electronic ground state of oxygen molecule are characterized by the N quantum number. The nuclear spin of ^{16}O oxygen atom is equal to zero and the electronic spin is equal to one. The first point explains why only odd values of the rotational quantum number N can exist and the second point leads to a splitting of the rotational levels for a given value of N into triplets corresponding to $J = N, N \pm 1$, where J is the quantum number related to the total angular momentum. The resulting rovibrational Raman selection rules are $\Delta N = 0, \pm 2, \Delta J = 0, \pm 1, \pm 2$ for the anisotropic scattering and $\Delta N = 0, \Delta J = 0$ for the isotropic scattering. In this work, we have been essentially interested in the polarized spectra (probe and pump beams polarized in parallel directions) of the normal fundamental Q branch ($\Delta N = \Delta J = 0, v = 0 \rightarrow 1$). From the selection rules we see that the polarized normal Q-branch contains both isotropic and anisotropic contributions.

In order to determine the influence of the anisotropic part on the width measurements of the polarized Q branch, we have recorded pure anisotropic spectra of oxygen at 295 K by crossing the field polarizations at a right angle. Our purpose was to determine experimental linewidths corresponding to the pure anisotropic contribution for a few N lines. We do not have any results for $N = 1$ and 3 due to the weakness of these lines as already reported by Hill *et al.*[23] in their study of the depolarization ratios of Q-branch triplets. Although the precision of our measurements is not very high, we will see (Sec. IV) that the anisotropic broadening coefficients are close to the coefficients obtained for the polarized Q branch. On the other hand, as the depolarization ratios of $Q(N)$ components are relatively small (1.8% for $N = 1$ to 4.9% for $N = 11^{23}$), the effect of the anisotropic part on the width measurements of the polarized Q branch is negligible. In other words, we can say that the measured

"polarized widths" are equal to pure isotropic widths. We have extended this conclusion to higher temperatures for pure O$_2$ and to the O$_2$–N$_2$ mixture.

In our study, the pressure limits have been chosen in order to minimize the effect of the splitting into triplets and Dicke narrowing at lower pressure and the effects of interferences between neighboring N components at higher pressure. With these conditions, we have assumed that each triplet can be represented by only one spectral component. In other words, the oxygen molecule has been treated with $^1\Sigma$ theory as the nitrogen molecule. This assumption is correct provided of course that the minimum pressure used is not too low. This minimum pressure was not arbitrarily chosen, but was found by fitting calculated spectra with $^3\Sigma$ theory to calculated spectra with $^1\Sigma$ theory at various pressures. That has been done at room temperature. The $^3\Sigma$ synthetic spectrum was obtained by taking into account each triplet component and also satellite lines around $Q(11)$ line. The frequencies were those given by Loëte and Berger[24] and the relative intensities were calculated from the isotropic and anisotropic contributions given by Loëte[24] and the average R value measured by Hill *et al.*[23] ($R = 0.717$). With this procedure it is really easy to study the error in the determination of the collisional width at a given pressure when a $^1\Sigma$ theory is used instead of the $^3\Sigma$ theory, and then the minimum pressure for which this error is not yet too large can be easily determined.

For the range of pressures considered here, the apparatus function has not been taken into account explicitly, because its contribution is very small. Indeed, this apparatus function is essentially due to the pump source and has been measured with a Fabry–Perot interferometer. It is nearly a Gaussian function with an half-width at half-maximum of 1.1×10^{-3} cm^{-1}.

For some pressure and temperature conditions, Dicke narrowing leads to a reduction of the Doppler width resulting from velocity changing collisions. In an exhaustive study of this phenomenon in N$_2$,[8] it has been demonstrated that a soft collision model such as the Galatry model[6] is very suitable in accounting for observed spectra in Dicke narrowing regime. The complex Galatry function can be expressed as follows:

$$\mathrm{CG}(x_N, y_N, z) = \frac{1}{\sqrt{\Pi}} \int_0^\infty d\tau \exp\left\{ ix_N \tau - y_N \tau \right.$$
$$\left. + \frac{1}{2z^2}(1 - z\tau - e^{-z\tau}) \right\}. \quad (1a)$$

The characteristic parameters appearing in this equation are given by

$$x_N = \frac{\omega - \omega_N - \Delta_N}{\gamma_D'}, \quad y_N = \frac{\Gamma_N}{\gamma_D'}, \quad z = \frac{\beta}{\gamma_D'},$$
$$\beta = \frac{kT}{2\Pi m D}, \quad \text{and} \quad \gamma_D' = \frac{\gamma_D}{\sqrt{\log 2}}. \quad (1b)$$

ω_N being the $Q(N)$ transition frequency, Γ_N the collisional half-width at half-maximum (HWHM), Δ_N the collisional shift, β the narrowing parameter or the effective frequency

of velocity-changing collisions, D the optical diffusion coefficient, and γ_D the Doppler width (HWHM). Let us specify that $\gamma_N = \Gamma_N/p$ represents the line broadening coefficient expressed in cm^{-1} atm^{-1}.

The optical diffusion coefficient can be estimated from the mass self-diffusion coefficient D_m (for O_2 $D_m = D_{m0} = 0.189$ cm^2 s^{-1} at $P_0 = 1$ atm and $T_0 = 273.15$ K^{25}). The variation of D_m as a function of pressure and temperature is given by[25]

$$D_m = D_{m0}\left(\frac{T}{T_0}\right)^{\alpha}\frac{P_0}{P}. \qquad (2)$$

The N_2 study[8] has demonstrated that the optical diffusion coefficient D is a fraction of D_m ($D \simeq \frac{2}{3}D_m$). On the other hand, the α coefficient has been found[8] ($\alpha = 1.5$). Since the mass self-diffusion coefficient and the inelastic collision rates of O_2 and N_2 are comparable, we have assumed for O_2 that $D \simeq \frac{2}{3}D_m$ and $\alpha = 1.5$. The influence of Dicke narrowing is characterized by the ratio of y_N to z_N[8,26] $[r_N = (y_N/z_N)]$. For O_2 and for temperatures between 295 and 1350 K, r_N ranges from 1.1 to 1.5, whereas the minimum value of y_N is 2.6 obtained for $N = 19$, $P = 303$ Torr, and $T = 769$ K. So, taking into consideration these limits of r_N and y_N, one can say that Dicke narrowing will have a small influence on the collisional width measurement.[8] For example, for the lowest value of y_N corresponding to the lowest pressure at 769 K for $N = 19$, the difference between the collisional widths obtained from the Galatry and Voigt profiles is 2.4% and is maximum. This difference decreases with increasing pressure. Since the line broadening coefficient for each $Q(N)$ line is obtained by applying a linear regression to a set of collisional linewidths obtained at different pressures ($\geqslant 300$ Torr), the difference in terms of line broadening coefficient comes to about 1%. Even though this difference is relatively small, it is of the order of the standard deviation on the line broadening coefficient and for that reason, we have used the Galatry profile to extract the collisional linewidths.

As described previously, in order to eliminate the effects of triplet splitting, our measurements were made at pressures above 300 Torr, and thereby minimizing the uncertainties resulting from models for Dicke narrowing. However, at these relatively high pressures, the effects of line interferences due to overlap between $Q(N)$ lines[10,27] become significant whatever the temperature. As a consequence, the assumption of an additive superposition of Galatry profiles (or Lorentz, or Voigt profiles) is not valid. From a perturbation theory, Rosenkranz has proposed a very simple model appropriate in the case of small overlap[9] and whose expression with reduced parameters is the following:

$$R(x_N,y_N,\eta_N) = \frac{1}{\pi}\frac{y_N - \eta_N x_N}{y_N^2 + x_N^2}, \quad \text{with } \eta_N = pY_N, \qquad (3)$$

where p is the pressure and Y_N the line mixing coefficient for the $Q(N)$ line related to the rate of rotational energy transfer from state N to $N'(W_{N'N})$ by

$$Y_N = 2\sum_{N' \neq N}\frac{W_{N'N}}{\omega_{N'} - \omega_N}. \qquad (4)$$

Let us mention that Eq. (3) can be also written as

$$R(x_N,y_N,\eta_N) = \frac{1}{\pi}(\text{Im } u_N - \eta_N \text{ Re } u_N), \qquad (5)$$

where

$$u_N = \frac{1}{x_N - iy_N}. \qquad (6)$$

This decomposition into individual Lorentz and dispersive components has the advantage of showing the possibility to simultaneously account for Dicke narrowing and line mixing effects through the following expression:

$$S(x_N,y_N,\eta_N,z) = \frac{1}{\pi}[\text{Re } CG(x_N,y_N,z) \\ - \eta_N \text{ Im } CG(x_N,y_N,z)]. \qquad (7)$$

This expression is a particular case of the more general expression given by Lavorel *et al.* valid whatever the amount of overlap.[28] Let us note that, in the low pressure limit when the line mixing disappears, the dispersive contributions do not contribute ($\eta_N = 0$) and Eq. (7) leads to the usual Galatry profile, which reduces itself to a Voigt profile when $z = 0$. The principal advantage of Eq. (7) is that it includes both Dicke effect and weak overlap, and is, consequently, correct whatever the pressure and temperature, providing that the Rosenkranz profile is a good representation of the line mixing. On the other hand, this equation is very simple and does not require a lot of computer time. So, instead of using different models (Lorentz, Voigt, Galatry, or Rosenkranz) whose choice, which depends on pressure and temperature, is somewhat arbitrary, we have preferred to use Eq. (7) for all the spectra. This procedure reduces the uncertainties inherent in the choice of the line shape model to extract the collisional linewidths. The band shape for the full Q branch is then simply the sum of the contributions given by each rotational line

$$I(\omega) = A\sum_N \rho(N)S(x_N,y_N,\eta_N,z) + B. \qquad (8)$$

The collisional widths are extracted by least-squares fit of Eq. (8) to the experimental Raman spectra. The linewidths Γ_N, the perturbed frequencies $\omega_N + \Delta_N$, the line mixing Y_N, the overall amplitude scale factor A and the constant base line offset B can be adjustable parameters in the fitting procedure. For each spectrum the narrowing parameter β has been fixed to the estimated value as explained previously

$$\beta = \frac{3kT}{4\pi m D_{m_0}(T/T_0)^{1.5}(P_0/P)}. \qquad (9)$$

The unperturbed frequencies ω_N and the populations $\rho(N)$ have been calculated from accurate spectroscopic constants.[11]

For most of the pressures considered, the line mixing was relatively weak, particularly for the high temperature spectra. So, it is always a little bit dangerous to unrestrainedly adjust the line mixing parameters Y_N. Therefore, in a preliminary analysis, all spectra have been fitted with a superposition of Voigt profiles, giving us a first set of line broadening coefficients. This set has been then inverted to obtain the inelastic rates of rotational energy transfer $W_{N'N}$, by using fitting laws such as the MEG model (see Sec. VII). The

$W_{N'N}$ elements have allowed us to estimate the mixing coefficients Y_N thanks to Eq. (4). This set of Y_N has been then used as initial input parameters in the least-squares fitting procedure using Eq. (8). These parameters have been freely adjusted whenever possible, for example at 295 and 446 K excluding $Q(1)$ which is too weak. At higher temperatures the Y_N have been contrained to stay close to their initial values. When the line mixing coefficients have been unrestrainedly adjusted there are relatively large uncertainties in their values. However, they seem to have a correct dependence vs the rotational quantum N, but we estimate that they cannot be confidently compared to values calculated from fitting laws [with Eq. (4)] and so they cannot test the ability of the various fitting laws to reproduce them.

In brief, the recording conditions of the fundamental $(v = 0 \rightarrow 1)$ Q branch of O_2 and O_2-N_2 are reported in Table I. For the O_2-N_2 collisional pair we have used air whose composition has been considered as 79% N_2 and 21% O_2.

IV. COLLISIONAL LINE BROADENING COEFFICIENTS

Notice that the line broadening coefficients of O_2-N_2 are deduced from the whole line broadening coefficients through the usual relation

$$\gamma_N = C_{O_2}\gamma_N(O_2 - O_2) + C_{N_2}\gamma_N(O_2 - N_2), \quad (10)$$

where C_{O_2} and C_{N_2} are the concentrations of O_2 and N_2, respectively. Similar equations obviously hold for the line shifting δ_N and line mixing $W_{N'N}$ coefficients.

The set of pressure broadening coefficients has been obtained from the fitting procedure described above, as a function of temperature for O_2-O_2 and O_2-N_2. The experimental data are reported in Tables II and III jointly with the O_2 CARS line broadening coefficients at 295 K from Ref. 5 for comparison. Our experimental values corresponding to the pure anisotropic contribution are also reported in comparison with pure rotational Raman linewidths.[29] Finally, we give also some results concerning the first and second hot band of pure oxygen ($v = 1 \rightarrow 2$ and $v = 2 \rightarrow 3$, respectively) at 1350 K. The uncertainties correspond to twice the standard deviation (2σ). At the lower temperatures, the uncer-

tainties are larger for the low-N transitions due to their weak intensities and partial overlap. It clearly appears from Table II that the agreement between the CARS data at 295 K[5] and ours is quite correct for all observed rotational lines. Let us mention that our data are more accurate. It is interesting to note that the N dependence of the self-broadening coefficients of oxygen follows the same pattern as for nitrogen[10] displaying similar resonance effects in the rotational population transfers. Furthermore, the values of the broadening coefficients of O_2-O_2 and N_2-N_2 are very close, meaning that oxygen and nitrogen collisions have about the same efficiency. So, it is not really surprising that the line broadening coefficients of the O_2-N_2 mixture (see Table III) are very close to those obtained for pure oxygen. Another intercomparison to other experimental Raman linewidths concerns the relations between isotropic and anisotropic linewidths. Let us note $W_{N'N}(v)$ the rate for an inelastic collision-induced energy transfer from rovibrational state (N,v) to rovibrational state (N',v). It results that the Raman line broadening coefficients for a transition from a state $i \equiv (N,v \cdots)$ to a state $j \equiv (N'',v'' \cdots)$ can be expressed in terms of the following approximation[30,31]

$$\gamma(i,j) = \frac{1}{2}[k_{inel}(i) + k_{inel}(j)] + \gamma_{elas}^{ori}(i,j) + \gamma_{elas}^{vib}(i,j)$$

$$\text{with } k_{inel}(i) = -\sum_{N' \neq N} W_{N'N}(v)$$

$$\text{and } k_{inel}(j) = -\sum_{N' \neq N''} W_{N'N''}(v''), \quad (11)$$

where k_{inel} are the total inelastic rates for rotational energy transfers in the initial v and final v'' vibrational states, γ_{elas}^{vib} the line broadening resulting from collision induced elastic vibrational dephasing assumed to be independent of rotational state and γ_{elas}^{ori} the line broadening arising from molecular reorientation. The last two columns of Table II represent the total linewidths of the Q branch of the first hot band ($v = 1 \rightarrow 2$) and second hot band ($v = 2 \rightarrow 3$) of O_2 at 1350 K. There are no significant systematic differences between these linewidths and the linewidths extracted at about the same temperature (1317 K) for the fundamental Q branch. So, we can assume that the rates for rotationally inelastic collisions are independent of the vibrational state. On this basis, the rates for rotational energy transfer are assumed to be equal in the lower and upper vibrational states. On the other hand, the extrapolation of this study at high pressure (a study which will be dealt with in another report[32]) has shown that pure vibrational dephasing is negligible for oxygen collisions. Let us recall that for an isotropic Raman Q branch the molecular reorientation contribution to the linewidths is identically zero and that a pure rotational spectrum has no vibrational dephasing. With the considerations mentioned above, Eq. (11) can be written as

$$\gamma_{(N)} = -\sum_{N' \neq N} W_{N'N} \quad (12)$$

for an isotropic Raman Q-branch transition and as

TABLE I. Recording conditions of the stimulated Raman Q branch of the collisional systems O_2-O_2 and O_2-N_2.

Collisional system	Temperature (K)	Pressure range (Torr)	N range
O_2-O_2		150–460	1–9
	295	150–1500	11–23
	446	240–920	1–21
	769	300–900	3–19
	990	760–1520	1–21
	1317	900–1530	3–29
	1350	760	39–55
O_2-N_2	295	740	1–21
	446	740	1–21
	990	740–1550	1–21

18 January 2024 21:35:04

TABLE II. Experimental O_2 self-broadening coefficients (HWHM in 10^{-3} cm^{-1} atm^{-1}). The uncertainties correspond to twice the standard deviation.

N	295 K	295 K[a]	295 K[b]	293 K[c]	446 K	769 K	990 K	1317 K	1350 K	1350 K[d]	1350 K[e]
1	53.6 ± 2.0	51.6 ± 4.6			40.0 ± 1.5		23.0 ± 1.2			15.9 ± 1.0	17.9 ± 1.5
3	47.7 ± 1.0	46.3 ± 1.9			36.7 ± 1.2	26.1 ± 0.5	20.7 ± 0.7	17.5 ± 0.9		16.4 ± 1.0	20.8 ± 1.5
5	45.3 ± 0.8	43.9 ± 1.6	50.9 ± 4.4	50.5	35.3 ± 1.2	24.3 ± 0.5	20.0 ± 0.7	17.9 ± 0.9		15.0 ± 1.0	19.8 ± 1.5
7	45.3 ± 0.8	43.7 ± 1.1	45.3 ± 3.9	49.0	32.5 ± 0.6	22.5 ± 0.5	19.8 ± 0.7	17.3 ± 0.9		15.9 ± 1.0	16.2 ± 1.5
9	42.6 ± 0.8	42.4 ± 1.7	51.3 ± 3.3	47.9	32.3 ± 0.6	22.7 ± 0.5	19.6 ± 0.7	16.6 ± 0.9		16.4 ± 1.0	15.6 ± 1.5
11	41.7 ± 0.8	40.9 ± 1.1	46.4 ± 4.5	45.7	31.5 ± 0.6	22.4 ± 0.5	19.6 ± 0.7			15.7 ± 1.0	15.7 ± 1.5
13	41.9 ± 0.8	40.4 ± 1.1			31.0 ± 0.6		18.7 ± 0.7	15.4 ± 0.9		16.2 ± 1.0	
15	38.8 ± 0.8	38.6 ± 1.7			30.7 ± 0.6	21.9 ± 0.5				16.9 ± 1.0	
17	38.0 ± 0.8	37.7 ± 1.2	40.3 ± 3.4	40.1	29.7 ± 0.6		18.5 ± 0.7	15.0 ± 0.9		15.7 ± 1.0	
19	36.1 ± 0.8				28.5 ± 0.6	21.4 ± 0.5				14.9 ± 1.0	
21	36.9 ± 0.8				28.3 ± 0.6		17.7 ± 0.7	14.5 ± 0.9		14.9 ± 1.0	
23	31.6 ± 1.4									14.4 ± 1.0	
25										14.4 ± 1.0	
27										13.3 ± 1.0	
29								13.2 ± 0.9		13.7 ± 1.0	
31										13.1 ± 1.0	
33										13.5 ± 1.0	
35										12.7 ± 1.0	
37										12.0 ± 1.0	
39									12.5 ± 1.0		
41									12.0 ± 1.0		
43									11.4 ± 1.0		
45									10.4 ± 1.0		
47									12.5 ± 1.0		
49									11.6 ± 1.0		
51									9.7 ± 1.0		
53									9.2 ± 1.0		
55									7.9 ± 1.0		

[a] Data from Ref. 5.
[b] Pure anisotropic linewidths.
[c] Experimental data from Ref. 29.
[d] First hot band.
[e] Second hot band.

$$\gamma_{(N,N+2)} = -\frac{1}{2}\left(\sum_{N' \neq N} W_{N'N} + \sum_{N'' \neq N+2} W_{N''N+2}\right) + \gamma_{elas}^{ori} \qquad (13)$$

for a pure rotational or a pure anisotropic Raman transition (case of an S transition).

The pure anisotropic linewidths reported in Table II (column 4) are in relatively good agreement with the pure rotational linewidths of Bérard *et al.*[29] (column 5). The differences observed between the anisotropic linewidths and the isotropic linewidths (columns 2 and 3) may give an estimate of the collisional reorientation contribution ($\gamma_{elas}^{ori} \simeq 4 \times 10^{-3}$ cm^{-1} atm^{-1} at room temperature for an average value over N).

V. COLLISIONAL LINE SHIFTING COEFFICIENTS

The line shifting coefficients have been obtained in a large temperature range for pure oxygen (up to 1317 K) and at two temperatures (295 and 446 K) for the O_2–N_2 mixture. The results are reported in Table IV as a function of the rotational quantum number N at each temperature. Figure 2 shows an example of line shift measurement for the oxygen–nitrogen mixture for the $Q(13)$ line at room temperature. The reference cell contains pure oxygen at a pressure corresponding to its partial pressure in the mixture. By applying the differential method explained in Sec. II, the frequency difference between the two lines gives the collisional shift for the corresponding pressure of nitrogen. By repeating the operation at other pressures, we have obtained the line shifting coefficients. Figure 3 illustrates the very good linear dependence of the shift vs pressure on the $Q(13)$ line at 446 K showing the quality of the measurements. The line *shifting* coefficients do not exhibit a clear variation vs rotational quantum number N and the mean values over N expressed in density units weakly depend on the temperature. Let us re-

TABLE III. Same caption as for Table II but for O_2 perturbed by N_2.

N	295 K	446 K	990 K
1	54.0 ± 4.0	43.0 ± 2.0	22.5 ± 2.0
3	47.5 ± 2.0	40.0 ± 1.5	22.0 ± 1.3
5	44.5 ± 2.0	37.1 ± 1.2	22.0 ± 1.0
7	45.0 ± 1.5	35.4 ± 1.2	20.5 ± 1.0
9	44.5 ± 1.5	34.7 ± 1.2	21.2 ± 1.0
11	44.0 ± 1.5	35.0 ± 1.2	19.4 ± 1.0
13	42.5 ± 1.5	34.0 ± 1.2	18.3 ± 1.0
17	42.0 ± 2.0	32.2 ± 1.2	17.7 ± 1.0
21	37.5 ± 2.0	30.9 ± 1.2	17.6 ± 1.0

TABLE IV. Experimental line shifting coefficients (in 10^{-3} cm^{-1} atm^{-1}) for O_2–O_2 and O_2–N_2 measured at low pressure. The uncertainties correspond to one standard deviation.

	295 K		446 K		990 K	1317 K
N	O_2–O_2	O_2–N_2	O_2–O_2	O_2–N_2	O_2–O_2	O_2–O_2
5		-3.3 ± 0.3		-1.5 ± 0.6	-2.0 ± 0.9	-0.7 ± 0.4
7		-4.0 ± 1.0	-1.8 ± 0.1	-2.1 ± 0.6	-0.7 ± 0.5	-1.4 ± 0.3
9		-2.9 ± 0.9	-1.5 ± 0.4	-2.2 ± 0.6	-1.9 ± 0.9	-0.7 ± 0.3
11		-3.8 ± 0.7		-2.5 ± 0.5	-2.2 ± 0.8	
13	-2.9 ± 0.3	-3.1 ± 0.5	-2.4 ± 0.1	-2.2 ± 0.7	-0.3 ± 0.5	-0.8 ± 0.6
15	-2.7 ± 0.3					
17	-3.5 ± 0.3	-5.4 ± 0.9	-3.0 ± 0.4	-1.5 ± 0.6	-0.6 ± 0.6	-0.5 ± 0.3
19	-2.3 ± 0.4					
21	-2.7 ± 0.5	-6.6 ± 1.3	-2.4 ± 0.2	-1.6 ± 0.6	-1.0 ± 0.7	-0.2 ± 0.3
Mean value in density units (mk amagat^{-1})	-3.1 ± 0.2	-3.8 ± 0.3	-3.5 ± 0.3	-3.3 ± 0.3	-3.4 ± 1.0	-3.4 ± 1.0

mark that the line shifts of pure oxygen are nearly the same as for the oxygen–nitrogen mixture.

VI. SEMICLASSICAL CALCULATION OF LINE BROADENING AND LINE SHIFTING PARAMETERS

The calculation of $Q(N)$ and $S(N)$ linewidths and line shifts has been done by means of a semiclassical theory[12] which has appeared convenient for various molecular systems in a large temperature range. This theory includes a nonperturbative treatment of the differential collision cross sections through the linked cluster theorem, and the effects of close collisions are accounted for, both in the intermolecular potential and in the classical trajectory description. The expression of the line broadening coefficients tied to an optical transition $i \rightarrow j$ is given by

$$\{\gamma(i,j) - i\delta(i,j)\}(\text{cm}^{-1})$$

$$= \frac{n}{2\pi c} \bar{v} \langle 1 - e^{-S_{2,ji}(b,\bar{v})} e^{i\eta_{ji}(b,\bar{v})} \rangle_{b,N}. \qquad (14)$$

In Eq. (14), $\gamma(i,j)$ and $\delta(i,j)$ are, respectively, the half-width (HWHM) and shift of the $i \rightarrow j$ line, n is the density of perturbers, $\bar{v}$ denotes the mean relative velocity, and the average is taken over the impact parameter b and the rotational quantum number N of the perturber.

Moreover, $S_{2,ji}(b,\bar{v})$ is the second order differential cross section accounting for anisotropic interactions and $\eta_{ji}(b,\bar{v})$ is a sum of two dephasing contributions, a first order one due to the vibrational dependence of the isotropic potential and a second order contribution related to the vibrational dependence of the quadrupole moment of the active molecule.[16] The intermolecular potential used in this theory is the sum of an atom–atom pairwise additive Lennard-Jones potential and of the quadripolar long range electrostatic interaction. The isotropic part of the potential is fitted to a Lennard-Jones shape with adjustable characteristic parameters ϵ and σ. The atom–atom and molecular parameters used in the calculation are given in Table V.

The calculated Raman $Q(N)$ line broadening coefficients are gathered in Table VI for pure O_2 (up to 1350 K) and in Table VII for O_2–N_2 (up to 2000 K). Some $S(N)$ line
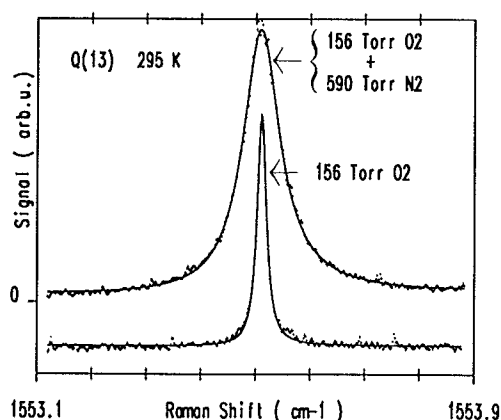
FIG. 2. Illustration of the line shift measurement with the two cells. The solid line is the fit of the theoretical profile [see Eq. (8)] to the experimental data.
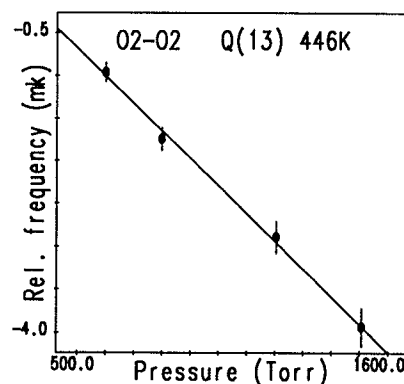

FIG. 3. Shift linearity vs pressure of O_2 (1 mk = 10^{-3} cm^{-1}).

TABLE V. Molecular parameters for O_2–O_2 and O_2–N_2 interactions

Atom–atom parameters[a]

$e_{oo} = 0.26 \times 10^{-10}$ erg Å^6/molecule;

$d_{oo} = 0.25 \times 10^{-7}$ erg Å^{12}/molecule

$e_{NN} = 0.25 \times 10^{-10}$ erg Å^6/molecule;

$d_{NN} = 0.29 \times 10^{-7}$ erg Å^{12}/molecule

Lennard-Jones parameters[b]

$\epsilon(O_2) = 120$ K; $\epsilon(N_2) = 97$ K

$\sigma(O_2) = 3.55$ Å; $\sigma(N_2) = 3.73$ Å

Quadrupole moments

$Q(O_2)^c = -0.39$ D Å; $Q(N_2)^d = -1.4$ D Å

Vibrational parameters for O_2[e]

$$\xi = \frac{r - r_e}{r_e} \frac{1}{\alpha} \frac{d\alpha}{d\xi} = 1.32 \frac{1}{Q} \frac{dQ}{d\xi} \simeq -2$$

$$(\langle 1|\xi|1\rangle - \langle 0|\xi|0\rangle) = 0.826 \times 10^{-2}$$

$$a_{01} = \frac{\dot{\alpha}}{\alpha}[\langle 1|\xi|1\rangle - \langle 0|\xi|0\rangle] = 1.09 \times 10^{-2}$$

$$b_{01} = 2\frac{\dot{Q}}{Q}[\langle 1|\xi|1\rangle - \langle 0|\xi|0\rangle] \simeq -3.3 \times 10^{-2}$$

[a] Reference 33.
[b] Reference 34.
[c] Reference 35.
[d] Reference 36.
[e] References 35, 37, and 38.

widths calculated at 295 K are also given in column 3 of Table VI. The calculated Raman $Q(N)$ line shifts are reported in Table VIII.

As expected, the most striking feature of these calculations is the closeness of line broadening coefficients between O_2–O_2 and O_2–N_2 pairs. This is clear from comparison of the O_2 and N_2 molecular parameters (see Table V). The two molecules are very similar except for their quadripolar moments. It is thus obvious that the O_2 broadening is dominated by short range forces. The good consistency obtained between experiment and theory especially at high temperature would permit a reliable prediction of line broadening parameters for temperatures higher than those experimentally attained and for broadening by other molecular gas species. Concerning line shift values, a good overall consistency is obtained between theory and experiment. However, as already stated,[16] the calculation of the shifts depends on an

TABLE VI. O_2 self-broadening coefficients (HWHM in 10^{-3} cm^{-1} atm^{-1}) calculated within the semiclassical theory of Ref. 12. Columns 2 and 3 refer respectively to $Q(N)$ linewidths and to $S(N)$ linewidths.

N	295 K[a]	295 K[b]	446 K	769 K	990 K	1317 K	1350 K
1	46.5	50.7	34.1	23.4	19.9	16.6	14.8
3	47.1		34.9	24.1	20.5	17.1	
5	44.9	45.8	33.8	23.7	20.3	17.0	15.2
7	43.5		32.8	23.2	20.0	16.9	
9	43.0	44.3	32.3	22.9	19.7	16.7	14.9
11	42.4		32.0	22.6	19.5	16.5	
13	41.7	43.1	31.7	22.5	19.4	16.4	14.6
15	40.6		31.2	22.3	19.3	16.3	
17	39.2	41.2	30.6	22.1	19.1	16.2	14.4
19	37.7		29.9	21.9	19.0	16.2	
21	35.9	38.9	29.0	21.6	18.8	16.0	14.3
23			28.1	21.2	18.6	15.9	
25				20.8	18.4	15.8	14.0
27				20.4	18.1	15.6	
29				19.9	17.8	15.4	13.7
33							13.3
37							12.9
41							12.4
45							11.8
49							11.2
53							10.6

[a] $Q(N)$ linewidths.
[b] $S(N)$ linewidths.

TABLE VII. O_2–N_2 broadening coefficients (HWHM in 10^{-3} cm^{-1} atm^{-1}) calculated within the semiclassical theory of Ref. 12.

N	295 K	446 K	990 K	1315 K	2000 K
1	41.5	31.2	19.1	16.2	12.8
3	43.8	32.5	19.8		
5	43.1	31.7	19.7	16.7	13.2
7	42.7	31.0	19.5		
9	42.5	30.5	19.5	16.5	13.1
11	42.3	30.3	19.1		
13	42.0	30.0	19.0	16.3	12.9
15	41.5	29.5	18.9		
17	40.9	28.9	18.8	16.1	12.8
19	40.3	28.0	18.6		
21	39.7	27.1	18.4	15.9	12.7
23			18.2		
25			17.9	15.6	12.6
27			17.6		
29			17.3	15.2	12.4
33				14.8	12.2
37				14.3	11.9
41					11.7
45					11.4
49					11.1
53					10.8

TABLE VIII. Line shifting coefficients (in 10^{-3} cm^{-1} atm^{-1}) calculated within the semiclassical theory of Ref. 12. (A): pure O_2; (B): O_2–N_2.

T		$N=1$	$N=5$	$N=9$	$N=13$	$N=17$	$N=21$
295 K	A	-4.0	-4.3	-4.5	-4.5	-4.4	-4.3
	B	-3.4	-3.8	-3.9	-3.9	-3.7	-3.5
446 K	A	-2.8	-2.9	-3.0	-3.0	-3.0	-2.9
	B	-2.4	-2.5	-2.6	-2.6	-2.6	-2.5
769 K	A	-1.7	-1.7	-1.8	-1.8	-1.8	-1.7
	B	-1.4	-1.5	-1.5	-1.5	-1.5	-1.5
990 K	A	-1.3	-1.3	-1.4	-1.4	-1.4	-1.4
	B	-1.1	-1.1	-1.2	-1.2	-1.2	-1.1
1317 K	A	-1.0	-1.0	-1.0	-1.0	-1.0	-1.0
	B	-0.8	-0.9	-0.9	-0.9	-0.9	-0.9

adjustable parameter y which accounts for the different vibrational dependences of the repulsive and attractive parts of the isotropic potential. Here the value $y = 2$ has been found for pure O_2 and assumed for O_2–N_2.

VII. FITTING LAWS

The experimental line broadening coefficients have been used to determine all elements of the relaxation matrix thanks to fitting laws. Among the various fitting laws, the modified exponential gap law[14] (MEG) is one of the most used. For this model the upward rate of transitions from N to N' (with $N' > N$) is described according to

$$-\,\mathrm{Re}\ W_{N'N} = \alpha \left(\frac{T}{T_0}\right)^{-N} \left(\frac{1 + aE_N/kT\delta}{1 + aE_N/kT}\right)^2$$
$$\times \exp(-\beta E_{N'N}/kT)\,, \qquad (15)$$

with $\alpha, N, \delta,$ and β the temperature independent parameters, T_0 a reference temperature, $E_{N'N} = |E_{N'} - E_N|$ the energy gap, and a is a constant proportional to the duration of a collision. The parameter a has been calculated from an estimation of distance of closest approach r_c obtained by equating the isotropic Lennard-Jones intermolecular potential to $\frac{3}{2} kT$ (cf. Ref. 28). This distance r_c is weakly temperature dependent. We obtained $r_c = 3.29$ Å for O_2–O_2 with $\sigma = 3.55$ Å and $\epsilon = 120$ K at $T = 295$ K leading to $a = 1.67$. The MEG model does not vary a lot with this coefficient (very small differences are observed when a ranges from 0.5 to 10). So, to simplify, we have used $a = 1.5$ for the O_2–O_2 and O_2–N_2 collisional pairs leading to exactly the same model as for pure nitrogen.

Another rate law, the energy corrected sudden law

(ECS) has also been developed these last years,[15,16] allowing the determination of all the elements of the relaxation matrix through the basis rate constants W_{OL},

$$\mathrm{Re}\ W_{N'N} = (2N' + 1)\exp[\,(E_{N'} - E_{N>})/kT\,]\,\Omega_{N>}^2$$
$$\times \sum_L \begin{pmatrix} N & N' & L \\ 0 & 0 & 0 \end{pmatrix}^2 (2L + 1)\Omega_L^{-2}\ \mathrm{Re}\ W_{OL}, \qquad (16)$$

where $N>$ is the greater of N and N' and Ω the adiabatic factor proportional to the characteristic interaction length l_c. A few fitting laws have been proposed to describe the basis rate constants. In the ECS-P model[16] the basis rates are taken as a power law,

$$-\,\mathrm{Re}\ W_{OL} = \frac{A_0 (T/T_0)^{-N}}{[L(L+1)]^\gamma}. \qquad (17)$$

In the ECS-EP model[13,17,39] the rapid decay of the rate constants at large $|\Delta N|$ is described by restricting the amount of angular momentum which can be transferred, using a hybrid form between a power law and an exponential law

$$-\,\mathrm{Re}\ W_{OL} = \frac{A_0 (T/T_0)^{-N}}{[L(L+1)]^\gamma} \exp\left(\frac{-\beta E_L}{kT}\right). \qquad (18)$$

The three models MEG, ECS-P, and ECS-EP have been tested for the collisional systems O_2–O_2 and O_2–N_2. In each case, the parameters of the models have been fitted to the whole set of experimental line broadening coefficients. The resulting parameters are given in Table IX. The standard

TABLE IX. Fitting parameters of the MEG, ECS-P, and ECS-EP models, obtained by inversion of Raman line broadening coefficients of O_2–O_2 and O_2–N_2. The reference temperature is $T_0 = 295$ K. σ is the standard deviation obtained for the whole set of data (all temperatures). Let us recall that 1 mk $= 10^{-3}$ cm^{-1}.

$T_0 = 295$ K		O_2–O_2	O_2–N_2
MEG	α	16.70 ± 0.20 mk/atm	17.00 ± 0.40 mk/atm
	N	1.32 ± 0.01	1.31 ± 0.01
	δ	1.32 ± 0.03	1.30 ± 0.05
	β	1.45 ± 0.03	1.41 ± 0.05
	σ	0.99	0.74
ECS-P	A_0	24.50 ± 0.80 mk/atm	23.00 ± 0.70 mk/atm
	N	1.01 ± 0.01	1.03 ± 0.02
	l_c	1.23 ± 0.09 Å	1.60 ± 0.20 Å
	γ	0.90 ± 0.01	0.87 ± 0.01
	σ	1.34	0.99
ECS-EP	A_0	19.08 ± 0.52 mk/atm	20.13 ± 0.62 mk/atm
	N	1.02 ± 0.01	1.04 ± 0.02
	l_c	4.26 ± 0.49 Å	3.86 ± 0.73
	γ	0.81 ± 0.01	0.81 ± 0.01
	β	0.056 ± 0.003	0.050 ± 0.002
	σ	1.11	0.79

deviation σ obtained for the whole set of line broadening coefficients (all temperatures for each collisional system) is of the order of 10^{-3} cm^{-1} atm^{-1} which is close to the experimental uncertainties. The MEG law seems to be the best model to reproduce these line broadening coefficients, ECS-

EP gives also excellent results and is a little bit superior to ECS-P. Experimental and theoretical data deduced from each model are compared on Figs. 4 and 5 for O_2-O_2 and O_2-N_2, respectively. It clearly appears that both rotational quantum number N and temperature dependences are well reproduced with the MEG and ECS-EP models. The results are somewhat different with the ECS-P model. Indeed, the experimental data for the highest rotational level and the lowest temperature is not very well reproduced and the mod-
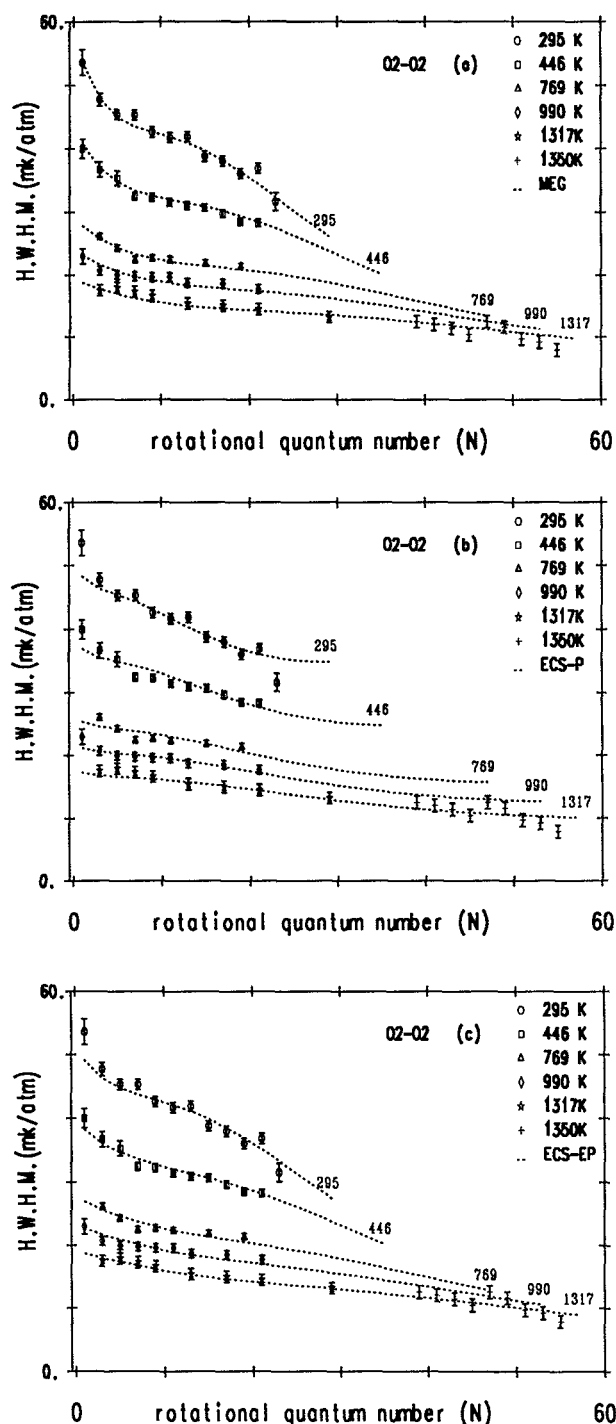
FIG. 4. Collisional broadening coefficients of O_2-O_2 as a function of rotational quantum number N at each temperature. The dotted lines are the MEG (a), ECS-P (b), and ECS-EP (c) broadening coefficients derived from the best fit parameters (see Table IX). Let us recall that 1 mk $= 10^{-3}$ cm^{-1}.
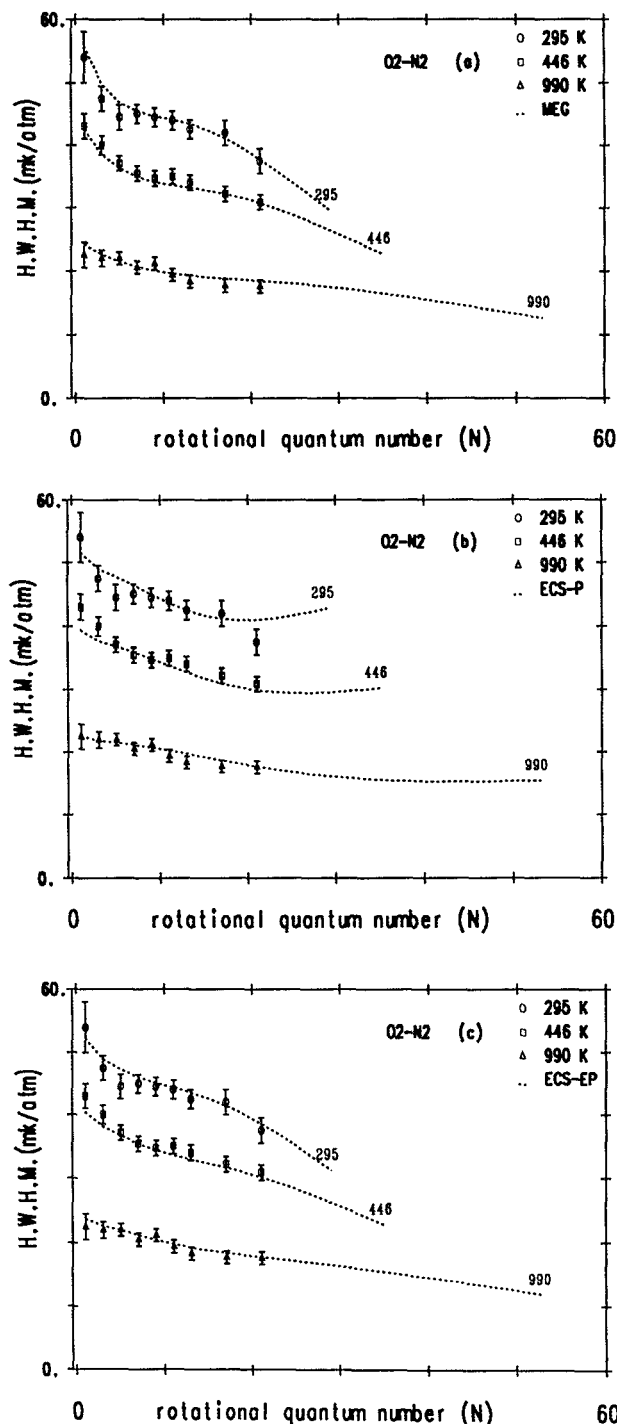
FIG. 5. Same caption as Fig. 4 but for the O_2-N_2 collisional system.

el predicts an increase of the broadening coefficients for higher rotational quantum number which is not physically reasonable for such collisional systems. But from a general point of view, the three models give similar results to reproduce the line broadening coefficients. So, we may conclude that the experimental line broadening coefficients are equally well characterized by either statistical or dynamical models. Accurate state-to-state rotational energy transfer measurements could be very useful to distinguish between several models. For example, very recently, Bonamy *et al.*[40] have reconsidered the ECS-EP scaling law in light of the state-to-state rate measurements reported for N_2.[41] They suggest replacing the adiabatic factor, given by De Pristo *et al.*[15] and used up to now in all ECS studies and in particular in this work, by an alternate expression. The new adiabatic factor has the object of eliminating unphysical behavior of the relaxation matrix in the modeling of the rotational angular momentum relaxation correlation function for high rotational quantum number. But such unphysical behavior at high N does not appear in the present study for the modeling of the line broadening coefficients.

Let us remark from Table IX that the best fit parameters of the fitting laws of the O_2-N_2 mixture are nearly the same as those obtained for pure oxygen.

VIII. CONCLUSION

As a conclusion, we can say that accurate line broadening, line shifting, and line mixing coefficients have been obtained for pure oxygen and for the oxygen–nitrogen mixture over a wide temperature range. The measured line broadening and line shifting coefficients have been compared to semiclassical calculations leading to an overall good agreement. Three relaxation models have been tested based either on statistical (MEG) or on dynamical (ECS-P and ECS-EP) fitting laws. The best results have been obtained with the MEG and ECS-EP rate laws. The best fit parameters of the fitting laws will allow us to calculate collapsed Q-branch spectra at high density. Comparison with observed high density SRS spectra will provide a critical test of the various fitting laws. This will be the subject of a future report. We may consider that the knowledge of collisions effects at low pressure of oxygen and nitrogen is now similar and we estimate that oxygen may be confidently used as the probe molecule in CARS thermometry.

ACKNOWLEDGMENTS

[1] D. A. Greenhalgh, in *Advances in Nonlinear Spectroscopy*, edited by J. H. Clark and R. E. Hester (Wiley, 1988), pp. 193–251.
[2] S. Fujii, M. Gomi, K. Eguchi, S. Yamaguchi, and Y. Jin, Comb. Sci. Tech. **36**, 35 (1984).
[3] T. Dreier, B. Lange, J. Wolfrum, and M. Zahn, Appl. Phys. B **45**, 183 (1988).
[4] W. R. Lempert, B. Zhang, R. B. Miles, and J. P. Looney, J. Opt. Soc. Am. B **7**, 715 (1990).
[5] Y. Ouazzany, J. P. Boquillon, and B. Lavorel, Can. J. Phys. **65**, 1588 (1987).
[6] L. Galatry, Phys. Rev. **122**, 1218 (1961).
[7] R. H. Dicke, Phys. Rev. **89**, 472 (1953).
[8] G. Millot, B. Lavorel, R. Saint-Loup, and H. Berger, J. Phys. (Paris) **46**, 1925 (1985); G. Millot, Thèse de Doctorat de Physique, Université de Bourgogne, 1986.
[9] P. W. Rosenkranz, IEEE Trans. Antennas Propag. **23**, 498 (1975).
[10] B. Lavorel, G. Millot, R. Saint-Loup, C. Wenger, H. Berger, J. P. Sala, J. Bonamy, and D. Robert, J. Phys. (Paris) **47**, 417 (1986).
[11] G. Rouillé, G. Millot, R. Saint-Loup, and H. Berger, J. Mol. Spectrosc. (submitted).
[12] D. Robert and J. Bonamy, J. Phys. (Paris) **40**, 923 (1979).
[13] T. A. Brunner and D. Pritchard, *Dynamics of the Excited State*, edited by K. P. Lawley (Wiley, New York, 1982), p. 589.
[14] M. L. Koszykowski, L. A. Rahn, R. E. Palmer, and M. E. Coltrin, J. Phys. Chem. **91**, 41 (1987).
[15] A. E. De Pristo, S. D. Augustin, R. Ramaswamy, and H. Rabitz, J. Chem. Phys. **71**, 850 (1979).
[16] L. Bonamy, J. Bonamy, D. Robert, B. Lavorel, R. Saint-Loup, R. Chaux, J. Santos, and H. Berger, J. Chem. Phys. **89**, 5568 (1988).
[17] G. Millot, J. Chem. Phys. **93**, 8001 (1990).
[18] J. Bonamy, D. Robert, J. M. Hartmann, M. L. Gonze, R. Saint-Loup, and H. Berger, J. Chem. Phys. **91**, 5916 (1989).
[19] G. Millot, B. Lavorel, R. Chaux, R. Saint-Loup, G. Pierre, H. Berger, J. I. Steinfeld, and B. Foy, J. Mol. Spectrosc. **127**, 156 (1988).
[20] R. Chaux, C. Milan, G. Millot, B. Lavorel, R. Saint-Loup, and J. Moret-Bailly, J. Opt. **3**, 19 (1988).
[21] M. L. Gonze, R. Saint-Loup, J. Santos, B. Lavorel, R. Chaux, G. Millot, H. Berger, L. Bonamy, J. Bonamy, and D. Robert, Chem. Phys. **148**, 417 (1990).
[22] Byschel and Dyer, Phys. Rev. A **33**, 3113 (1986).
[23] R. A. Hill, P. Esherick, and A. Owyoung, J. Mol. Spectrosc. **100**, 119 (1983).
[24] M. Loëte and H. Berger, J. Mol. Spectrosc. **68**, 317 (1977); M. Loëte, Thèse de Doctorat de Physique, Université de Bourgogne, 1976.
[25] W. Jost, in *Diffusion in Solids, Liquids, Gases*, edited by E. Hutchison and P. Van Rysselberghe (Academic, New York, 1960).
[26] P. L. Varghese and R. K. Hanson, Appl. Opt. **23**, 2376 (1984).
[27] G. J. Rosasco, W. Lempert, W. S. Hurst, and A. Fein, Chem. Phys. Lett. **97**, 435 (1983).
[28] B. Lavorel, G. Millot, R. Saint-Loup, H. Berger, L. Bonamy, J. Bonamy, and D. Robert, J. Chem. Phys. **93**, 2185 (1990).
[29] M. Bérard, P. Lallemand, J. P. Cebe, and M. Giraud, J. Chem. Phys. **78**, 672 (1983).
[30] A. E. De Pristo and H. Rabitz, J. Quantum Spectrosc. Radiat. Transfer **22**, 65 (1979).
[31] G. J. Rosasco, A. D. May, W. S. Hurst, L. B. Petway, and K. C. Smyth, J. Chem. Phys. **90**, 2115 (1989).
[32] G. Millot, C. Roche, R. Saint-Loup, J. Santos, R. Chaux, and H. Berger (to be published).
[33] M. Oobatake and T. Ooi, Prog. Theor. Phys. **48**, 2132 (1972).
[34] Fitted to the spherically averaged atom–atom potential.
[35] D. E. Stogryn and A. P. Stogryn, Mol. Phys. **11**, 371 (1966).
[36] F. Mulder, G. Van Dijk, and A. Van der Avoird, Adv. Mol. Phys. **39**, 407 (1980).
[37] M. A. Buldakov, B. V. Korolev, I. I. Matrosov, and T. N. Popova, Opt. Spektrosk. **62**, 519 (1987); **62**, 758 (1987).
[38] D. W. Oxtoby, D. Levesque, and J. J. Weis, J. Chem. Phys. **68**, 5528 (1978).
[39] S. L. Dexheimer, M. Durand, T. A. Brunner, and D. E. Pritchard, J. Chem. Phys. **76**, 4996 (1982).
[40] L. Bonamy, J. M. Thuet, J. Bonamy, and D. Robert, J. Chem. Phys. (in press).
[41] G. O. Sitz and R. L. Farrow, J. Chem. Phys. **93**, 7883 (1990).

18 January 2024 21:35:04